

GT2011-46846

STUDY OF THE FLOW OVER WIND TURBINE BLADE

R.S. Amano^{*}
Department of Mechanical Engineering
University of Wisconsin at Milwaukee

Ryan J. Malloy[†]
Department of Mechanical Engineering
University of Wisconsin at Milwaukee

ABSTRACT

This paper presents the comparison of the performance between two different designs of wind turbine blades; one is a straight and the other with a backward swept blade. The straight edge blade was constructed so that it is optimal on coming wind and rotation speeds with 7m/s and 20rpm. The blade has a length of 20m and uses a constant airfoil cross section NACA 4412. The swept edge blade has the same characteristics as the straight edge except for the trajectory of the edge. Each cross section has the same dimensions and has at the same distance from the hub as its corresponding section in the straight edge blade. To test this new design the performance of both blades were measured using CFD at a wind speeds ranging 0 to 20m/s. Comparisons were made for power generation and acoustic noise for both designs of the blades.

INTRODUCTION

Wind power has been shown to be one of the most viable sources of renewable energy. This is largely due to recent technological advances that have lowered the price of wind energy to a level that is competitive with more conventional means of producing energy. The blades of a wind turbine are an important component of the machine and thus have been the subject of much research. Most commercial blade designs incorporate a straight edge span wise profile with airfoil cross sections of various sizes and orientations. The configuration of these parameters usually follows guild lines resulting from well established theory. If these blades are designed correctly they can be very efficient. In an effort to increase this efficiency, some manufacturers have experimented with different profile geometries. One common alteration that has been seen is a swept edge profile, such as that found in the Skystream 3.7 turbine [1]. The advantages and disadvantages associated with this shape are not well documented due to the complex nature

of airflow around a rotating blade and the numerical investigation that is required.

Traditionally, analytical methods employing the blade element momentum (BEM) theory have been used to analyze wind turbine blade performance [2]. The BEM theory treats a given cross section of a turbine blade as an independent airfoil. Based on the rotation rate, oncoming wind speed and span wise position of the cross section, an appropriate chord length and angle of twist can be specified. Once several cross section configurations are specified, the overall performance of the blade can be estimated by indexing previously determined 2D lift, drag and moment data. These methods are efficient and reasonably accurate for an initial design but since each cross section is considered independent and the data used to determine its performance is 2D in nature, complex 3D flow effects are not directly taken into account [3]. For this reason many researchers have look to computational fluid dynamics to supplement their design process.

Bak et al. [4] explored the possibility of extracting force data from CFD simulations to supplement existing 2-D airfoil data. This data could then be used with the blade element momentum theory or actuator blade approach to analytically determine wind turbine performance. The turbine used in the simulations of this study is the NTK500/41 with LM19.1 blades [5]. The computational domain consisted of a third of the flow volume of the entire rotor taking advantage of the symmetry at every 120° interval. With this approach only a single blade needs to be simulated. The CFD simulation setup is shown in Fig. 1.

The CFD simulation set up used by Bak, et al. [4] has since been widely used to study flow dynamics about wind turbine blades. A similar approach was used by Sorensen [5] in an effort to better model the transition from laminar to turbulent flow conditions on the blade surface. This was done by first

^{*} ASME Fellow

[†] ASME Student Member

carrying out some 2D computations at a finite number of cross sections along the blade. The output of these computations was then used in the 3D flow computations. The 3D computational domain consisted of a third of the flow volume for a typical rotor and contained a single blade. The domain extended 6 radii up and down stream of the rotor and a y^+ of 2 was maintained at the blade surface.

Since the efforts of Sorensen [5] much of the CFD research of wind turbine blades has been used to study blade geometry alterations whose effects aren't able to be captured by analytical methods or whose effects on the flow field are not well understood. Johansen and Sorensen [6] used CFD to study tapered and swept tip geometries at different wind speeds and determined that the swept tip stalled at lower angles of attack than the tapered tip which maintained aerodynamic loads at higher angles of attack. A similar study was done by Ferre and Munduate [7].

NOMENCLATURE

C	rotor blade chord length
r	radial coordinate
R	Rotor blade radius
U_τ	friction velocity ($U_\tau = (\tau_w/\rho)^{1/2}$)
x	streamwise coordinate
y	distance from wall
y^+	non-dimensional distance from wall ($y^+ = U_\tau y/\nu$).
Greek symbol	
ν	kinematic viscosity of air
ρ	air density
τ_w	wall shear stress

MODELS OF WIND TURBINE BLADES

Straight Edge Blade

Wind turbine blade profiles are often constructed using the Blade Element Momentum theory (BEM). This theory will produce the angle of twist and chord length for a given airfoil cross section and rotation speed at a finite number of positions along the span of the blade. From these two dimensional sections a three dimensional shape can be extruded. The BEM theory accomplishes this by treating a given cross section as an independent airfoil which processes wind with a speed and direction that is a vector sum of the on coming wind speed and the wind speed generated by rotation. Since the direction and magnitude of the wind generated by rotation changes as a function of span wise position, the chord length and angle of attack of the airfoil cross sections must change as well. The BEM theory is not entirely accurate if the data for the airfoil cross sections that are used have not been corrected for rotational motion. It is for this reason that CFD analysis is necessary for new blade designs. CFD does not use predetermined airfoil data to predict the blade performance but instead solves the governing fluid flow equations at thousands

of positions on and around the blade in an iterative process. This approach allows the model to take into account any span wise wind velocity component which BEM theory cannot.

It was this method that was used to construct a straight edge blade prototype whose optimal on coming wind and rotation speeds were 7m/s and 20rpm. The blade has a length of 20m and uses the constant airfoil shape NACA 4412. Since no corrected NACA 4412 data was available, the blade performance will be measured using CFD at a wind speed of 10m/s.

Swept Edge Blade

In addition to the straight blade mentioned in the preceding subsection, a swept edge blade was tested. This swept edge blade has the same characteristics as the straight edge except for the trajectory of the edge. Each cross section has the same dimensions at the same distance from the hub as its corresponding section in the straight edge blade. The reason for testing this new geometry is that the straight edge blade is constructed using a formulaic approach which treats the airflow over the blade as perfectly perpendicular to the leading edge and neglects any span wise component. The swept edge blade profile aims to accommodate the span wise velocity component and delay the stall point of the rotor. This geometry has largely been investigated using the CFD approach. Recently an investigation into the loading and dynamic behavior of a swept blade was published by Larwood and Zureck [8]. They used codes developed by the National Renewable Energy Laboratories (NREL) which used a more analytical approach. A CFD approach is more suitable for this investigation since it is purely an aerodynamic study and CFD yields very accurate results which are quantitative as well as qualitative.

NUMERICAL METHODS

The geometries, computational domains, and meshes for the swept-edge and the straight blades were constructed in a similar manner. The blade geometries were first constructed in Pro-E CAD program using the sweep/blend function. Due to an axi-symmetric nature of the blade performance, only a single blade was required for 120 degree segment from each turbine simulation. The boundary for each segment is set as periodic type, so that the outgoing flow condition is used as an incoming one. In this way, the entire rotor section is physically covered. The surrounding volume was constructed easily with GRIDGEN's drawing capability.

A diffuser shaped domain was chosen with a 120 degree slice taken lengthwise along the axis. As mentioned earlier, each side of the domain was given periodic boundary conditions. The front and top planes were given as velocity inlets. The rear plane was given as a pressure outlet. The domain extended 5 diameters upstream of the blade and 10 diameters downstream of the blade. The domain had a radial height of 5 diameters at the front and 8 diameters at the back.

Several different mesh schemes were used in an effort to both resolve the boundary layer surrounding the blade and hub and obtain a computationally feasible domain. A $R \times 0.2R$ rectangle was constructed around the blade.

A start size of 0.05m was used at the surface of the blade along with a growth rate and maximum size of 1.3 and 0.5 extending into the rectangular volume. The wedge containing this rectangle and the rest of the blade/hub was meshed with a constant density mesh of 0.5m. The rest of the domain was given a growth rate of 1.08 and maximum size of 10 extending from this wedge.

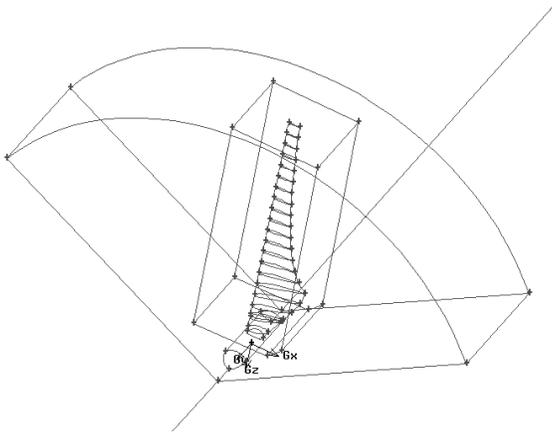


Figure 1: Boundary Layer Resolution Approach

For the swept blade the rectangle was modified slightly to accommodate the geometry. This approach is based off of the work done by Mandas et al. [9]. The final mesh contained 1.7 million elements.

The computations were made employing a finite volume method with SIMPLE algorithm in-house code (ANSYS). This code is based on a finite-volume approach with line-by-line iteration used for solving each transport equation, where both vector and scalar modes are co-located. The inlets were given an undisturbed velocity vector of 7m/s in the axial direction with a set turbulence level. It is to be noted that any set turbulence level is to be altered in the course of iteration process of the computations due to a nature of the periodic boundary condition. The sides of the wedge were designated as rotational periodic boundaries. Finally the fluid being chosen as a moving reference frame was given a rotational speed of 2.09rad/s. The turbulence closure model used was the $\kappa-\omega$ SST model. This model was used with success in a similar application by Ferrer and Munduante [10]. All results were obtained with convergence criteria of the normalized variable with the maximum order of 10^{-5} . Acoustic noise was evaluated using a separate code that incorporates Energy Efficient Transport (EET) model [11] and Farassat's formula [12] which is easier to get the noise signal than the Ffowcs Williams – Hawkins equation [13, 14].

As can be seen, the domain is quite large compared with the blade and hub. This is because the wake produced by the

turbine extends far downstream and it is not desirable for it to extend into the rear boundary. The volume extends 550m downstream and 100m up stream of the blade. These dimensions are based on previous work [4]. The radius of the front face is 100m while the back is 130m. The angle between the two side surfaces is 120° . This means that exactly 1/3 of the wind turbine will be modeled. This is done for computational efficiency. The computational methods that make this possible are explained in the following sections.

Mesh generation is an important part of this investigation and proved to be the most time-consuming. All meshes were done in GRIDGEN, the pre processor to FVM. As in most CFD investigations, a fine mesh is needed near areas of interest to accurately resolve flow conditions while a coarser mesh is needed elsewhere to maintain computational efficiency [15]. For this analysis, the area of interest is the region surrounding the aerodynamically active portion of the blade. This portion extends from 2m above hub to the tip of the blade. The meshing technique employed used both a structured and unstructured mesh. A structured mesh was used in the area surrounding the blade, as shown in Fig. 2.

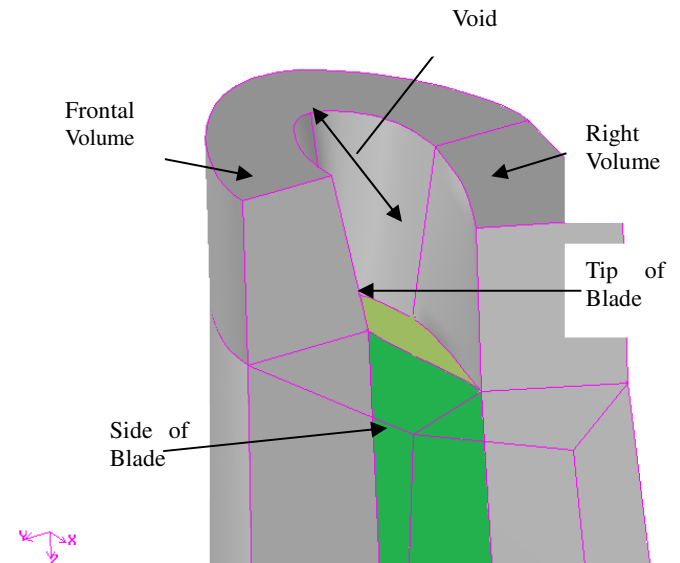


Figure 2: Mesh Scheme for Volumes Surrounding Blade

An unstructured mesh was used to represent the rest of the flow domain, as shown in Fig. 3.

The structured mesh was used for the region near the blade surface as it yields more accurate results due to its superiority of capturing viscous effect in the near-wall region, while, the unstructured mesh was employed in a outer region where the flow is mostly vortex and/or potential flow. Since the only area of interest is the area surrounding the blade, a structured mesh was only used here. The mesh parameters insured that $0.3 \leq y^+ \leq 5$ with an average of about 2, which is adequate boundary layer resolution, as shown by other researchers [4].

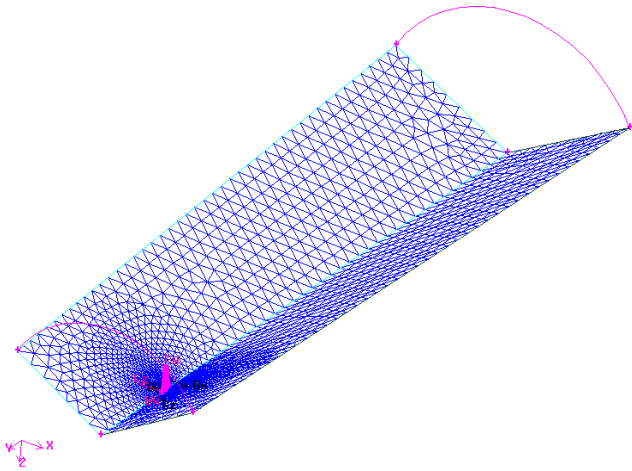


Figure 3: Flow Volume Mesh Density

RESULTS

In order to verify the computational results of the straight and swept edge blade, the computational results of the commercially available LM19.1 blade is qualitatively and quantitatively compared to results predicted by theory as well as published experimental performance data. In Fig. 4 the axial velocity in the flow field of the turbine is plotted on a plane intersecting the blade. This plane was then mirrored 120 degrees to show a full cross sectional view of the flow field. As can be seen the velocity of the air at positions far from the rotor are undisturbed and exhibit the specified oncoming wind speed of 20 m/s. In the region in front of the rotor and in the wake of the rotor it can be observed that the air has slowed down. This is in accordance with what is predicted by theory. The air slows down in front of the blade because it is striking a solid surface. The air in the wake of the turbine is slower than the free stream velocity because energy has been extracted from it by the turbine. These results show the right boundary conditions were chosen to accurately simulate free stream flow and the rotational motion of the turbine.

Figure 5 shows pressure contour plots on the upwind tip of the LM19.1 blade for an oncoming wind speed of 20m/s. From Fig. 5 the high pressure gradients at the leading edge can be observed. This is the expected location of the stagnation point and is the reason such a dense mesh is used in this area.

Figure 6 demonstrates the pressure contours that occur during the stall condition. At 20m/s the airflow cannot follow the contour of the blade and so separation occurs near the trailing edge resulting in decreased lift. This phenomenon is shown in that high pressure regions extend from the trailing edge to the leading edge forming irregular, jagged pressure contours indicative of the chaotic recirculating flow. The presence of this behavior shows that the boundary layer resolution and thus y^+ value are adequate.

In Fig. 7 the predicted performance of the LM19.1 by the simulation is compared to experimentally published performance data. Each simulation point represents a separate simulation with an inlet boundary condition corresponding to the specified oncoming wind speed. For both the experimental and simulation data the rotational speed was kept constant at 27.1 rpm. As can be seen there is good agreement between the results. The stall condition that occurs after 15m/s oncoming wind speed is accurately simulated. There is negligible difference between the simulation points and the experimental data with about 1-2% error except at 15m/s oncoming wind speed where the discrepancy is about 10%. This is at the threshold of stall and the flow conditions that exist are difficult for the turbulence model to define. However this discrepancy occurs only at point in a wind speed range of 0-20m/s, which is acceptable at this point given the accuracy of the rest of the simulation. This high degree of agreement shows the results of these simulations and those of the straight and swept edge blades can be trusted with a high degree of confidence.

In Fig.8 the result of a grid independence check is depicted. Numerical solutions are never exact but only an approximation. The values of the solution change as the grid density changes. The denser the grid the more accurate the results will be because the flow volume will be more accurately represented. However there is a point where the solution does not change appreciably with an increase in mesh density. It is important to identify this point for the results to be trusted. The mesh for the LM19.1 blade was adjusted 3 times and the solutions were compared. The predicted power outputs for an oncoming wind speed of 20m/s are reported in Fig. 8 and are indicative of the rest of the simulation results for the corresponding mesh densities. As can be seen for a 160% increase in number of nodes from trial 2 to 3 only a 1.5% change in the solution results. It can therefore be assumed that the mesh density used in trial 2 is adequate. After the adjustment, it was confirmed that the maximum y^+ for all the computations resides within 1.

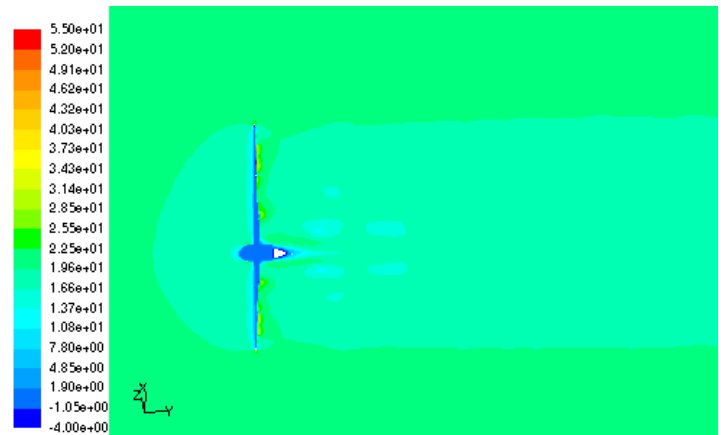


Figure 4. Axial Velocity in the Flow Field of Wind Turbine with LM19.1 Blades at Oncoming Wind Speed of 20m/s (units in m/s)

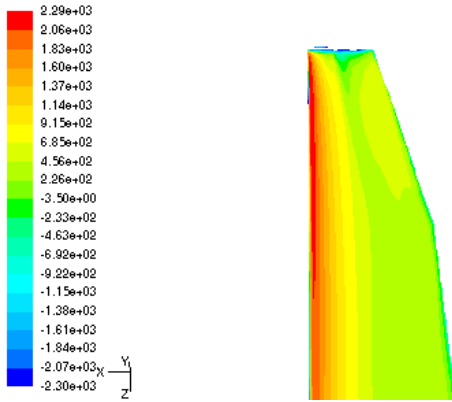


Figure 5. Pressure Contours at the Tip of the Upwind Side of the LM19.1 Blade at Oncoming Wind Speed of 20m/s (units in Pa)

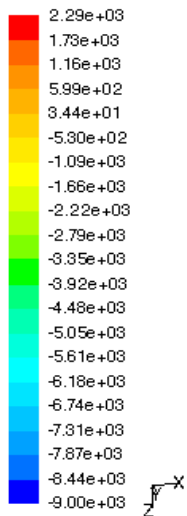


Figure 6. Pressure Contours on the Downwind Side of the LM19.1 Blade at Oncoming Wind Speed of 20m/s (units in Pa)

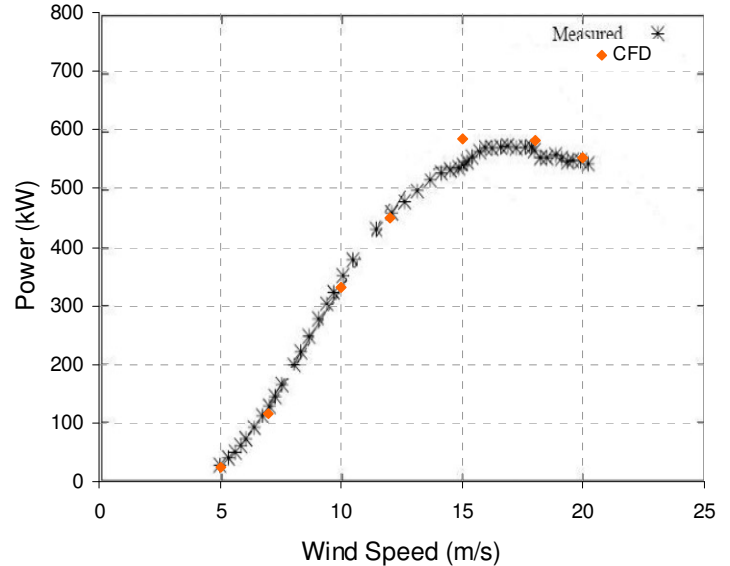


Figure 7. CFD Power Output Prediction Comparison for NTK500/41 Wind Turbine with LM19.1 Blades

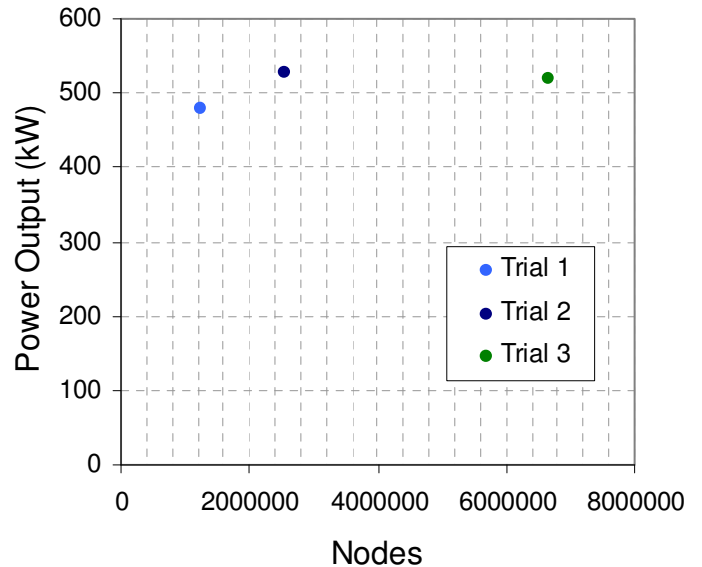


Figure 8. Grid Independence Check Using Power Output Prediction for NTK500/41 Wind Turbine with LM19.1 Blades at 20m/s Oncoming Wind Speed

In Figs. 9 and 10 it is clear that the straight blade out performs the swept blade due to the low pressures maintained along the majority of the blade surface for a wind speed of 20m/s. At the leading edge lower pressures are achieved by the straight edge blade on the pressure side of the blade which more than compensate for the higher stagnation point pressure. Along the trailing half of the blade it can be observed that lower pressures on the downwind side and slightly higher pressures on the upwind side are maintained by the straight edge blade as

opposed to the swept edge blade. The lower overall pressures on the straight edge blade produce more lift than on the swept edge which allows it to perform better at higher wind speeds. The same trend is found at $r/R=0.75$ from the hub as shown in Fig. 10. There is a smaller deviation between the two distributions which is expected given the fact that leading edge geometries at this location are more similar than they are at the tip.

In Figs. 11 and 12 the local pressure distributions are reported at an oncoming wind speed of 7m/s. They exhibit the similar trends as the pressure distributions at 20m/s except the magnitudes are much smaller. Clearly both turbines are more efficient at this wind speed due to the large difference in low and high pressures. In Fig. 11 it appears that overall lower pressures are achieved by the swept edge blade. The swept edge blade has considerably lower stagnation pressure and maintains a slightly lower pressure from 0.25 to 0.5 of the chord length. The local pressure distributions at 7m/s oncoming wind speed at $r/R=0.75$ from the blade reported in Fig. 12 are almost identical for the same reasons they were in Fig. 10. The only noticeable deviation between the two occurs during the leading half of the pressure side of the blade where lower pressures are maintained by the straight edge blade which is opposite of the behavior in Fig. 11. This suggests that lower portions of the straight edge blade produce more torque at 7m/s wind speed. The higher torque at these levels however does not compensate for the difference in torque generation at the tip of the blade. This is demonstrated by the overall higher power output by the swept edge blade at this wind speed as shown in Fig. 20.

The difference in performance of the two blades at high wind speeds may be attributed to higher tip loss for the swept edge design. At higher wind speeds the air starts to travel vertically up the blade as well as across it. If the blade edge is swept, more air may pass over the tip or even the leading edge of the blade than if the blade edge was straight. Since the lift is generated from air flowing over the airfoil cross section it is expected that the swept blade produce lower power at higher wind speeds.

In Figs. 13 through 16 locally generated aerodynamic noise by the blade surfaces at $r/R=0.95$ and 0.75 from the hub are presented for selected oncoming wind speeds. From Fig. 13 it is observed that the straight blade generates about 4-6% higher noise throughout the chord near the tip section in comparison with the swept blade except in the region close to the leading edge (about $x/C=0.2$) for the approaching wind of 20m/s. This sudden drop in the noise for straight blade in the near-leading edge section seems to be attributed to a fact that there is a much higher flow acceleration occurring in the straight blade this particular point in comparison with the swept blade, in which the incoming wind flow is directed in both chord direction and the radial direction resulting in lower flow acceleration. However, it is clear that near the tip, the swept edge blade produces less overall noise than does the straight edge blade. This trend can be attributed to the fact that less turbulence is being generated near the tip for swept blade than for the straight

blade, as discussed earlier. If we look at the mid span at $r/R=0.75$ (see Fig. 14), the noise level is low in both blades except for the straight blade it shows peak noise in the leading edge. The only difference worth noting is the spike of noise generation near the leading edge of the straight edge blade at a wind speed of 20m/s shown in Fig. 14. This trend corresponds to the higher pressure level at this point for the straight blade than for the swept blade. Similar trends are found for an oncoming wind speed of 7m/s as shown in Fig. 15. Then noise generated by the blade surface at a distance of $r/R=0.75$ from the hub is almost identical for both blade geometries as illustrated in Figs. 14 and 16. This behavior shows that the swept edge blade produces less noise than a straight edge blade in all locations and wind speeds.

Figure 17 shows the comparison of the overall noise between straight and swept blades as a function of wind speed. It is clear that swept blade reduces the noise by 5-10% over the straight blade. In Fig. 18 acoustic power generation and turbulent kinetic energy generation are plotted along a vertical line extending just off the trailing edge of the straight edge blade at an oncoming wind speed of 20m/s. One obvious feature is that the turbulence level varies fluctuating fashion along the blade span. This is an indication of a high flow oscillation occurring along the blade. Figure 19 shows the same plot but for the swept edge blade. Since the blade is curved, constructing the plot line along the trailing edge was challenging and does not correspond to the same position in space as the straight edge blade plot line. Therefore a direct comparison between the two cannot be made. However both show that there is a direct correlation between turbulent kinetic energy and acoustic power generation. Furthermore, it is clear that the distribution of turbulence is less chaotic along the swept blade in comparison with the straight blade. It may also be noticed that both the turbulent kinetic energy and sound generation plots are sinusoidal in nature.

Figure 20 shows the comparison of the overall power generation between straight and swept blades. As shown in this figure, the swept blade gains power approximately 10% higher than the straight blade up to the wind speed 12m/s. However, the trend completely reverses beyond the wind speed 13-15m/s. For higher wind speed the straight blade gains power about 20-30% higher than the swept blade. This is mainly attributed to the fact that a swept blade causes much less flow separation for the approaching wind speed less than 12m/s, while the flow separation occurs for both types of the blade for a higher wind speed. Under the wider flow separation region, a straight blade sustains the power more than a swept blade as the difference in the pressure between the suction and the pressure sides are larger for a straight blade than for a swept blade as evidenced in Figs. 9 and 10 for the wind speed 20m/s. The overall pressure difference, however, is still higher for a swept blade than a straight blade for a lower approaching wind speed (7m/s) as shown in Figs. 11 and 12.

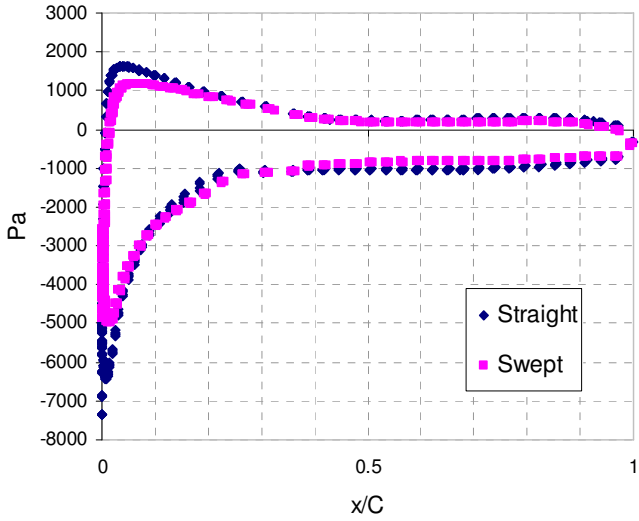


Figure 9. Local Pressure Distribution at $r/R=0.95$ from the Hub at 20m/s Oncoming Wind Speed

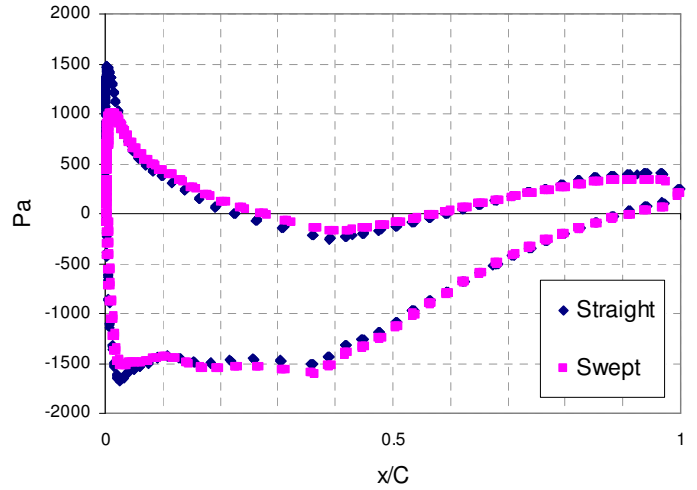


Figure 11. Local Pressure Distribution at $r/R=0.95$ from the Hub at 7m/s Oncoming Wind Speed

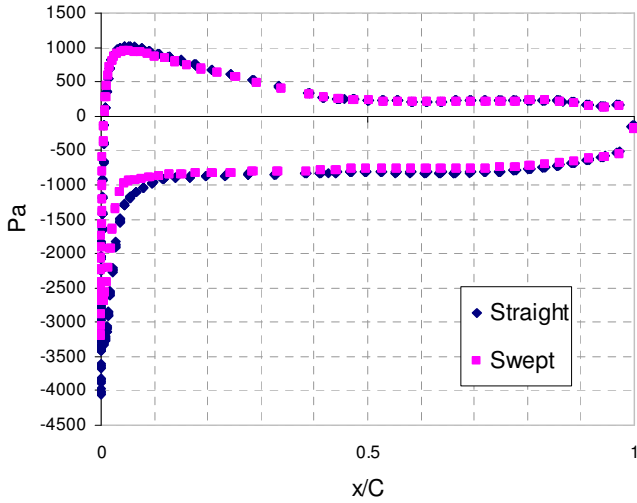


Figure 10. Local Pressure Distribution at $r/R=0.75$ from the Hub at 20m/s Oncoming Wind Speed

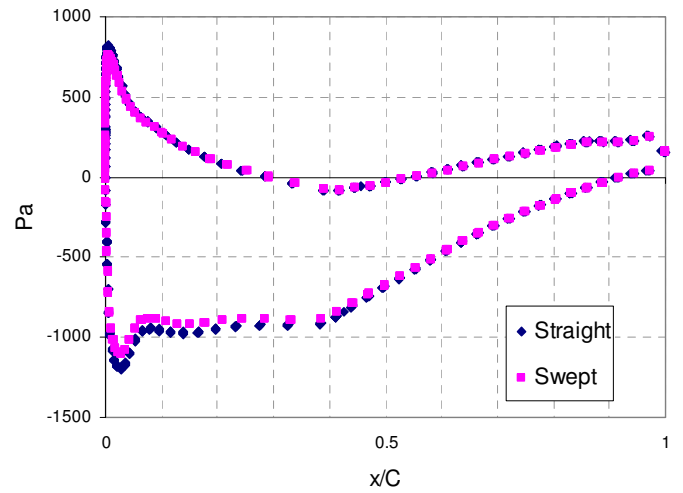


Figure 12. Local Pressure Distribution at $r/R=0.75$ from the Hub at 7m/s Oncoming Wind Speed

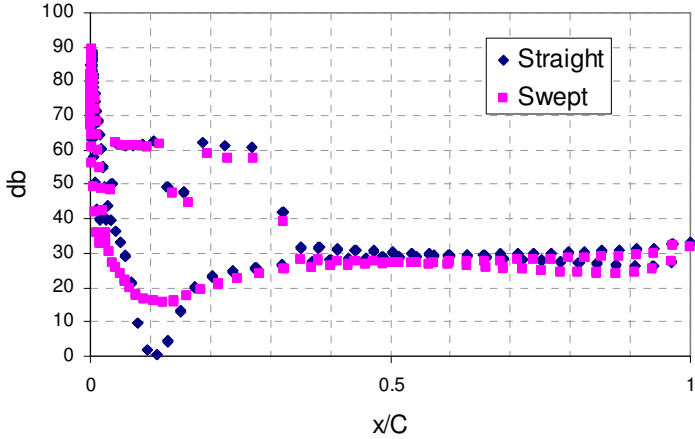


Figure 13. Local Noise Generation at $r/R=0.95$ from the Hub at 20m/s Oncoming Wind Speed

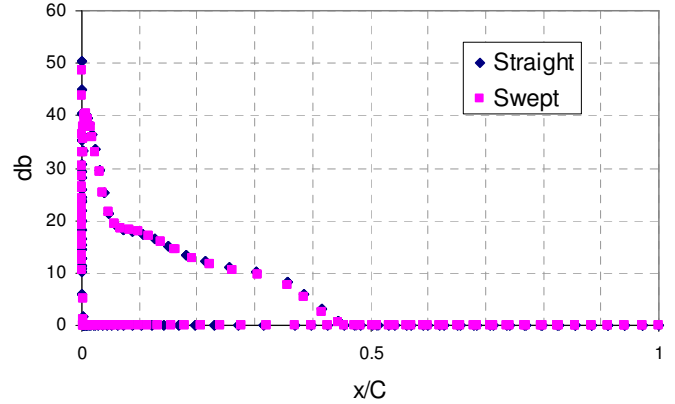


Figure 16. Local Noise Generation at $r/R=0.75$ from the Hub at 7m/s Oncoming Wind Speed

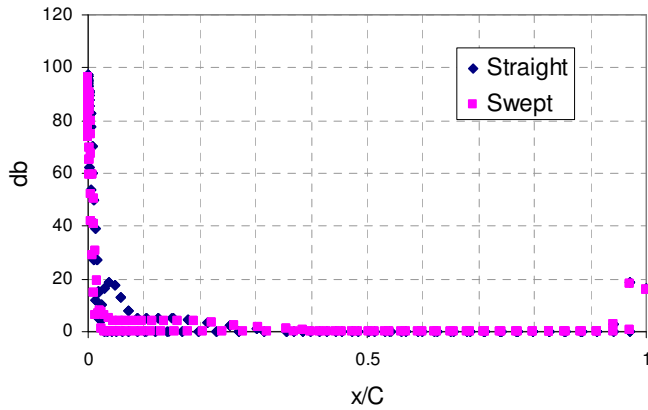


Figure 14. Local Noise Generation at $r/R=0.75$ from the Hub at 20m/s Oncoming Wind Speed

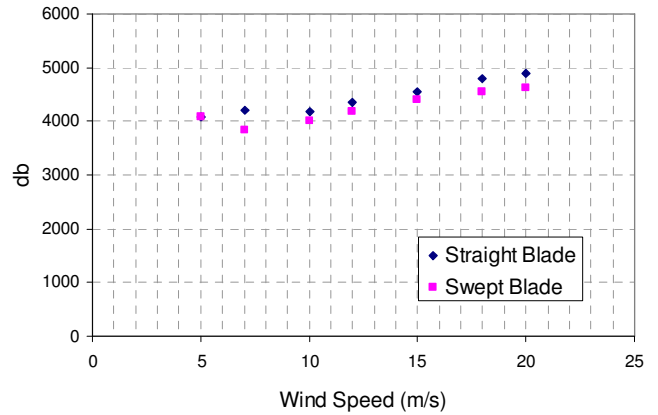


Figure 17. Overall Sound Generation

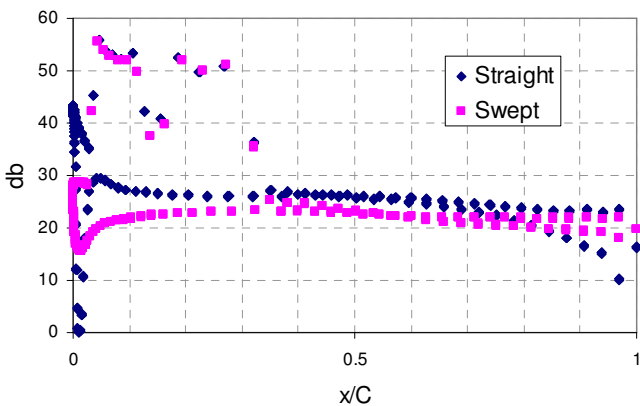


Figure 15. Local Noise Generation at $r/R=0.95$ from the Hub at 7m/s Oncoming Wind Speed

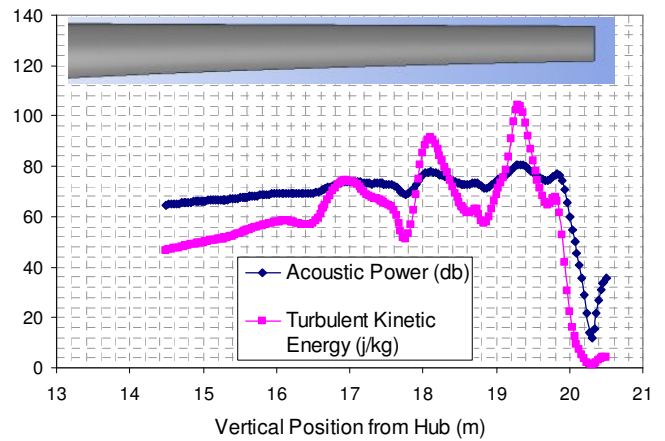


Figure 18. Acoustic Power and Turbulent Kinetic Energy Generation Comparison at 20m/s oncoming wind speed

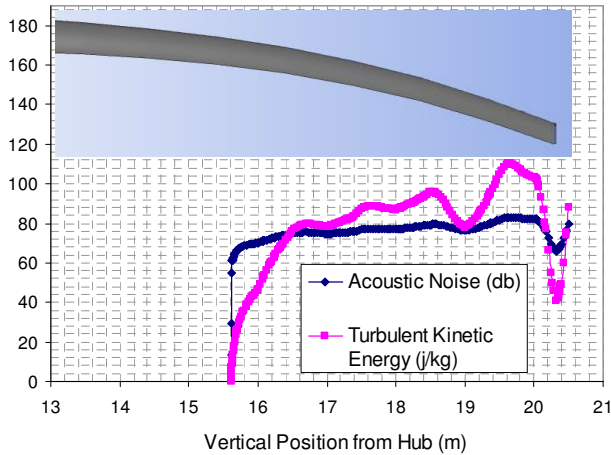


Figure 19. Acoustic Power and Turbulent Kinetic Energy Generation Comparison at 20m/s oncoming wind speed

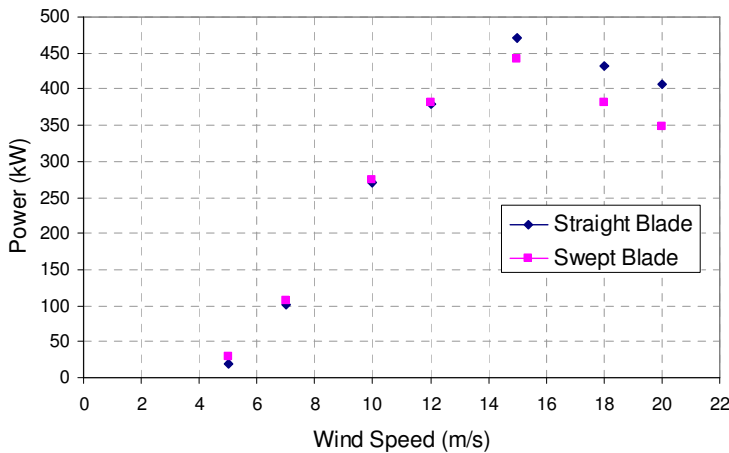


Figure 20. Overall Power Generation

CONCLUSION

The following conclusions emerged from this study:

1. A swept blade gains power over a straight blade by 10% in a wind speed range 0-12m/s.
2. Beyond the wind speed of 15m/s, a straight blade gains power as high as 20% more, whereas a straight blade might suffer with stall around the wind speed 15-20m/s.
3. A straight blade shows noise level 2-10% lower than a swept blade over a wide range of wind speed, and this trend does not seem to depend on a wind speed itself.
4. Acoustic power generation and turbulent kinetic energy generation do not correspond to the same position in space along the span-wise turbine blade.

And both blades show that there is a direct correlation between turbulent kinetic energy and acoustic power generation and they behave sinusoidal in nature.

5. The turbulence variation is much higher along the span for the straight blade and the swept blade, and this trend might be attributing to the higher noise in the straight blade.

Future work will include running more trials at different wind speeds and with different degrees of sweep. It is of interest to better understand how the swept edge design affects torque generation at the stall point. It is generally accepted that a swept tip will delay the stall point but to what degree and its relation to the degree of sweep is unknown. Also changes in the airfoil cross section at different positions along the blade itself to try an optimize performance. This is typically done with commercial blades such as the LM19.1 which uses three different cross sections. Finally a simple loading and fatigue analysis will be done to determine the loads at the hub/blade interface. One issue with blades designed for low wind speeds is that they experience high stresses from occasional high wind speeds that maybe found in a storm for example. These conditions will impact the blade geometry.

There are other methods that are used for optimizing blade performance that were not investigated here but should be mentioned. One of the most obvious strategies is to increase the diameter of the rotor because the swept area will contain more energy that can be abstracted. However this can be problematic as the loads at the hub/blade interface will increase dramatically. Research on relieving these loads through blade twist has been done by Larwood and Zuteck [8]. Rotors are also designed to have a high rotational speed. The more times the rotor moves through the swept area the more energy it can extract. Research has also been done on different near hub blade geometries by Mandas et al. [9]. Through a CFD study they found that if the blade taper was extended to the hub in stead of having a cylindrical connection that a 5% increase in power is possible. This new design does not have the potential to give an as strong structural interface connection as a cylindrical connection but with new materials are introduced this feature will have more applicability. Tip geometry has also been explored. CFD was used by Ferrer and Munduante [10] to explore the effect of a square tip, swept back tip and pointed tip whose point lies on the pitch axis on radial flow in the span wise direction. It was concluded that the tip geometry does affect the flow up the blade and that the pointed tip that lies on the pitch axis performed the best out of the three.

ACKNOWLEDGMENTS

This research is partially supported by US DOE DE-EE0000545 and We Energies. The program monitors from We Energies are Mr. Carl Siegrist and Ms. Amy Flom. Thanks are due to Mr. M. Brien for his dedicated assistance to the study of wind turbine blades.

REFERENCES

- [1] Southwest Windpower., www.windenergy.com
- [2] Vermeer, L., Sørensen, J., Crespo, A., 2003 "Wind Turbine Wake Aerodynamics" Progress in Aerospace Science; Vol. 39; 467-510.
- [3] Hansen, MOL., 2000 "Aerodynamics of Wind Turbines. Rotors, Load and Structures"; James&James, London
- [4] Bak, C., Fuglsang, P., Sorensen, N., Madsen, H., Shen, W., Sorensen, J., 1999 "Airfoil Characteristics for Wind Turbines" Riso-R-1065(EN)
- [5] Sørensen, N.N., 2002, "Transition Prediction on the NORDTANK 500/41 Turbine Rotor," Risø-R-1365, Risø National Laboratory, Roskilde.
- [6] Johansen, J., and Sorensen, N., N., 2002 "Numerical Investigation of Three Wind Turbine Blade Tips" Technical Report. Riso-R-1353(EN), Riso National Laboratory
- [7] Ferre, E., Munduate, X., 2005. "Wind Turbine Blade Tip Comparison Using CFD" Journal of Physics: Conference Series 75 (2007) 012005
- [8] Larwood, S. and Zuteck, M., 2006, "Swept Wind Turbine Blade Aeroelastic Modeling for Loads and Dynamic Behavior", Windpower 2006.
http://www1.pacific.edu/~slarwood/documents/Larwood_Windpower_2006.pdf
- [9] Mandas, N., Cambuliand, F., and Carcangiu, C., 2006, "Numerical Prediction of Horizontal Axis Wind Turbine Flow," University of Caglaira, EWEC 2006, Athens, Business, Science, and Technology.
- [10] Ferrer, E. and Munduante, W., 2007., "Wind Turbine Blade Tip Comparisons Using CFD." Journal of Physics Conference series, **75**, 012005
- [11] Khorrami, M.R., Singer, B.A., Berkman, M.E., "Time-Accurate Simulations and Acoustic Analysis of Slat free-Shear Layer," AIAA2001-2155, 7th AIAA/CEAS Aeroacoustics Conference, Maastricht, Netherlands.
- [12] Ffowcs Williams, J. E., and Hawkings, D. L., "Sound generation by turbulence and surfaces in arbitrary motion," Philosophical Transactions of the Royal Society of London, Series A, Vol. 264, 1969, 321~342
- [13] J. E. Ffowcs Williams and D. L. Hawkings, "Sound Generation by Turbulence and Surfaces in Arbitrary Motion," Philosophical Transactions of the Royal Society of London. Series A, Mathematical and Physical Sciences, Vol. 264, No. 1151 (May 8, 1969), pp. 321-342
- [14] Farassat, F., and Succi, G. P., "The prediction of helicopter rotor discrete frequency noise," Vertica, Vol. 7, 1983, 309~320
- [15] Bertagnolio, F., Sorensen, N., Johansen, J., Fuglsang, P., 2001 "Wind Turbine Airfoil Catalogue" Riso-R-1280(EN) Riso National Laboratory, Roskilde